First-Principles Molecular Dynamics Simulations of H_2O on α-Al_2O_3 (0001)

K. C. Hass* and W. F. Schneider

Ford Research Laboratory, SRL MD-3028, Dearborn, Michigan 48121-2053

A. Curioni and W. Andreoni

IBM Research Division, Zurich Research Laboratory, 8803 Rüschlikon, Switzerland

Received: January 5, 2000; In Final Form: April 13, 2000

We present a more detailed account of our recently reported [Hass, K. C.; Schneider, W. F.; Curioni, A.; Andreoni, W. *Science* **1998**, *282*, 265] first-principles molecular dynamics investigation of the static and dynamical behavior of adsorbed H_2O on α-Al_2O_3 (0001). Al-terminated surfaces with varying degrees of H_2O coverage are modeled using large periodic supercells. A predicted large relaxation of the clean surface agrees well with previous density functional theory calculations. Both molecular and dissociative H_2O adsorption modes are identified, with the latter favored by ∼10 kcal mol^{-1}. Complementary Al_8O_{12} cluster results are shown to be unreliable because of their finite lateral extent. Constrained dynamical calculations of free-energy barriers indicate that the dissociation rate is very high, even in the absence of defects, but differs by 3 orders of magnitude for two equally exothermic pathways (proton transfer being more favorable *across* a six-membered ring than to the nearest O site). Unconstrained simulations at intermediate H_2O coverages exhibit (1) spontaneous unimolecular and (2) H_2O-mediated dissociation events, as well as (3) the diffusion and hydrogen bonding of physisorbed H_2O and (4) an additional proton transfer reaction between adsorbed H_2O and OH species. An experimentally observed decrease in H_2O binding energies with coverage is explained in terms of a separation into defect-dominated, intrinsic (0001) terrace, and "hydrogen-bonding" regimes, with reasonable quantitative agreement throughout. Calculated O−H vibrational frequencies are consistent with known trends on aluminas but indicate a discrepancy between experimental observations for α-Al_2O_3 (0001) and models based on simple hydroxylation. Simulations for high H_2O coverages suggest the possibility of more complicated behavior, including the interchange of adsorbed and lattice oxygen and the etching of surface Al. A "fully"-hydroxylated α-Al_2O_3 (0001) surface in which each surface Al is replaced by three protons to give uniform OH-termination, as in aluminum hydroxides, is the most likely result of prolonged exposure. Results for this surface confirm its anticipated stability, provide a reasonable explanation of observed vibrational spectra, and reveal a complex, dynamical structure with extensive intraplanar hydrogen bonding.

1. Introduction

The current understanding of metal−oxide surfaces lags far behind that of most other solids.[1−4] Experimental studies are complicated by difficulties in preparing stoichiometric single-crystal surfaces, by charging effects during analysis, and by the sheer complexity of bulk and surface oxide structures. Theoretical progress has also been slow because of the limited data available for building and testing models and because of complications associated with the mixed ionic/covalent nature of the bonding, with long-range electrostatic, polarization, and relaxation effects,[5] and with the absence of a soft, norm-conserving pseudopotential[6] for O. These problems are further compounded for the surfaces of transition-metal oxides by strong correlation effects and associated metal−insulator transitions and magnetism.[1]

Alumina (Al_2O_3) surfaces are among the most important but least well understood of any metal oxide. Crystalline and amorphous aluminas[7,8] play significant roles in many prominent areas of science and technology. As major components in the earth's crust, they have long been of interest in geology and environmental sciences.[9] They are widely used as catalysts and catalyst supports,[10,11] as structural ceramics,[12] and as high-thermal-conductivity dielectric supports and substrates in electronic and optoelectronic devices.[12] Controlled and uncontrolled surface oxides on metallic Al are also important in many aspects of adhesion, corrosion, and tribology.[13] These latter areas are of growing concern in the automobile industry because of the increasing use of lightweight Al alloys in place of steel to improve fuel economy.[14] Aluminas are even believed to play a role in stratospheric ozone depletion through their effects as particulates in rocket exhaust.[15]

A major obstacle to understanding the "intrinsic" surface properties of aluminas (and most other metal oxides) is the ubiquitous presence of hydrogen.[3,10,11,16−20] Molecular H_2O and surface hydroxyl groups are generally present because of either the incomplete devolution of H_2O from aluminum hydroxide [$Al(OH)_3$] or aluminum oxy-hydroxide [AlOOH] precursors[7,8] or the adsorption of H_2O from the environment.[15(a),21−30] The stability of nominally stoichiometric γ-Al_2O_3 and other transitional phases may, in fact, depend on the existence of hydroxyl groups on internal pore surfaces[31] and possibly throughout the bulk.[32] The more stable α phase (corundum) has a simpler, hydrogen-free interior,[7,8] which makes it a more convenient starting point for fundamental surface studies of aluminas. The

* To whom correspondence should be addressed.

10.1021/jp000040p CCC: $19.00
Published on Web 05/19/2000

α-Al_2O_3 (0001) basal surface, in particular, has been extensively investigated,[15,20,33−58] although many questions remain about the effects of residual hydrogen and adsorbed H_2O. Most previous theoretical studies of this surface have either considered only an ideal, hydrogen-free termination[41,43−45,48−55] or have employed small cluster models[46,56−58] or empirical force fields[47(b),56,59] of unknown accuracy.

Recently, we have begun to examine[60] the behavior of H_2O on α-Al_2O_3 (0001) using the superior theoretical framework provided by first-principles (Car-Parrinello) molecular dynamics[61,62] (CPMD) with large, periodic supercells. This approach combines the accuracy and predictive power of density functional theory (DFT),[63] within a planewave pseudopotential formalism,[64] with the richness and flexibility of dynamical simulations of realistic surface models. CPMD and related methods have yielded unprecedented insights into a wide variety of complex chemical and materials systems and phenomena.[65] Initial applications to oxide surface chemistry have focused primarily on the binding of H_2O and other adsorbates to low-index surfaces of MgO,[66−70] TiO_2,[71,72] and other rocksalt[73] and rutile[71(a)] materials. Our recent extension[60] to the more complex α-Al_2O_3 (0001) surface elucidated many of the static and dynamical properties of adsorbed H_2O (including key surface reactions) at different coverages and provided a consistent interpretation of available experimental data. The present paper provides a more detailed account of that work and presents some analogous results for small cluster models of α-Al_2O_3 (0001), which highlight some of the pitfalls of the cluster approach.

2. Computational Details

Static and dynamic calculations for both supercell and cluster models were carried out on IBM RS6000 SP computers (with up to 32 nodes) using version 2.5 of the parallelized CPMD code developed by J. Hutter and copyrighted by IBM, Armonk, New York. Except for a few test cases, discussed in section 3A, the generalized-gradient-approximation (GGA) exchange-correlation functional of Becke−Lee−Yang−Parr[74,75] (BLYP) was employed. This particular functional was chosen because of its success[76] in reproducing experimental properties of liquid H_2O and because of the improved accuracy of GGA chemical bond energies relative to local density approximation (LDA) predictions.[77] Norm-conserving, nonlocal pseudopotentials for Al and O were generated by the Troullier−Martins procedure[78] in the separable Kleinman−Bylander representation;[79] s and p components were constructed for O using a cutoff radius of 1.05 au, and s, p, and d components were constructed[80] for Al using a cutoff radius of 1.80 au. A local analytic pseudopotential was assumed for H and was represented by a softened Coulomb potential with core and cutoff radii of 0.25 and 0.94 au, respectively. Electron wave functions were expanded in plane waves with energies up to 70 Ry. This cutoff was found to yield adequate convergence of relative energies, as in earlier work with a similar O pseudopotential.[76]

The specific supercell and cluster models considered are defined in subsequent sections. The large size of our supercells and the strongly insulating nature of α-Al_2O_3 allowed us to restrict Brillouin zone sampling to $\boldsymbol{k} = 0$ without significant loss of accuracy. Calculations for isolated clusters were performed using a cubic box, 13 Å or more on a side, with periodic image effects removed.[81] Standard iterative techniques (e.g., direct inversion in the iterative subspace (DIIS)) were used for static wave function[82] and geometry[83] optimizations. Some cluster atoms were frozen in position, as specified in section 3B, but all supercell atoms were free to relax.

Dynamical simulations employed a velocity Verlet integrator[84] with conservative options that ensured close proximity to the Born−Oppenheimer surface; these options consisted of a low fictitious electron mass (400 au), a short time step (4 au = 0.097 fs), and the artificial substitution of D for H to reduce the coupling between electronic and ionic degrees of freedom.[76] All ions were treated classically because of the currently prohibitive cost of path-integral molecular dynamics simulations for large systems.[85] This neglect of nuclear quantum effects is unlikely to affect any qualitative conclusions, but it does introduce quantitative uncertainties in the description of H_2O dissociation reactions in view of the large zero-point energy of H (or D) and the low barrier heights predicted.[86] Dynamical simulations were performed either with the energy conserved or with the temperature controlled by a Nosé−Hoover chain thermostat.[87,88] The latter was used only in sections 3C and 5B and with a sufficiently low thermostat frequency (750 cm^{-1}) to avoid coupling to O−H stretching modes. The frequencies of such modes were calculated from the power spectra of appropriate velocity−velocity autocorrelation functions, with the peak positions rescaled by 1.412 to correct for the fictitious electron mass and H → D substitution; this scale factor is not simply $\sqrt{2}$, but was extracted from preliminary calculations of the asymmetric stretching mode in isolated H_2O and D_2O. Lagrange multipliers were introduced in some of the constant-temperature simulations to determine the average forces to constrain particular bond lengths.[84,89] These forces were subsequently integrated to calculate free energy profiles along corresponding reaction paths[90,91] (section 3C).

3. Clean Surfaces and Low H_2O Coverages

Bulk α-Al_2O_3 has the corundum structure, with each O atom four coordinated to Al, each Al atom six coordinated to O, and the O sublattice nearly hexagonally close packed.[7] The Al and O atoms form distinct layers along the [0001] direction in the sequence ···Al−O_3−Al−Al−O_3−Al···. We assume, as in most previous studies,[41−60] that in the absence of H and adsorbed H_2O the α-Al_2O_3 (0001) surface is terminated by a single Al layer. Classical[47,59] and quantum[45] calculations agree that this termination is lowest in energy, primarily because it ensures the absence of an electrostatically unfavorable surface dipole moment.[92] Termination of nominally H-free (0001) surfaces by single Al layers has recently been confirmed experimentally,[20,36,52] although one cannot rule out the possibility that other surface compositions (e.g., O termination) may be favored by different preparation conditions.[35,40,93]

A. Static Supercell Calculations. Most of our calculations for clean and H_2O-covered α-Al_2O_3 (0001) employ a standard supercell approach, i.e., the surface is modeled by a two-dimensional periodic slab, which alternates with a suitable vacuum region along the [0001] direction. To increase accuracy and allow the study of longer-ranged surface phenomena (e.g., migration of H_2O), we construct supercells with much larger in-plane periodicities than in previous models[43,44,47−55] for α-Al_2O_3 (0001). Specifically, we choose a lateral cross section that corresponds to a 3×3 hexagonal surface cell, 14.244 Å on a side. In most cases, we also assume a 14.244 Å repeat distance perpendicular to the surface, with about equal thicknesses of slab and vacuum. Prior work[48] on α-Al_2O_3 (0001) and the comparisons below to thicker slab calculations[53,55] confirm the adequacy of these choices.

For a clean Al-terminated surface, we consider a slab with nine atomic layers (three O layers), for a total of 135 atoms (54 Al + 81 O) per supercell. Top and side views of a single

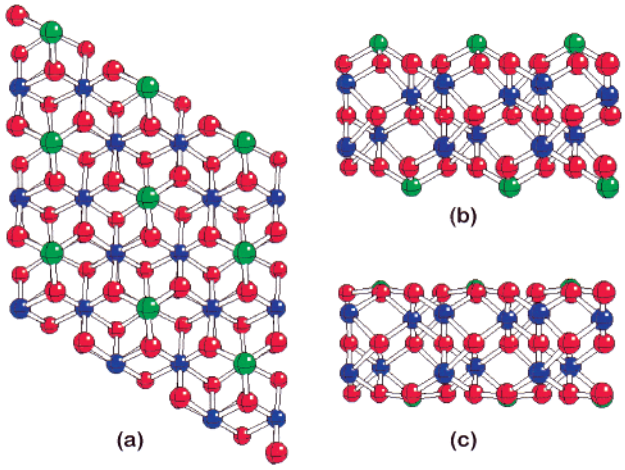

Figure 1. Top (a) and side (b) views of atoms within a single supercell for unrelaxed α-Al_2O_3 (0001) and side view (c) after relaxation. Hexagonal surface region has 3×3 periodicity compared to underlying primitive cell. Green, blue, and red spheres represent surface Al, interior Al, and O, respectively, with sphere diameters decreasing with distance.

cell in this model, with atoms in their unrelaxed bulk positions, are shown in Figure 1a and b, respectively. Each surface Al (green) in the unrelaxed structure has three O neighbors at 1.852 Å, while each interior Al (blue) has three similar O neighbors, plus three additional O neighbors at 1.963 Å. Atoms in the outermost O layers are also undercoordinated, with one long and two short bonds to neighboring Al, as opposed to two of each in the interior. Before relaxation, the distance between adjacent Al and O layers is 0.838 Å, and that between adjacent Al layers is 0.484 Å.

Upon relaxation, the outermost Al atoms move toward the surface, ending up almost in the outermost O plane, as shown in Figure 1c. This effect, and related structural changes that extend to much deeper layers, are by now well known,[43,44,47−55] although quantitative details are still controversial.[20,36,40] Table 1 lists the present predictions for the percent changes in spacings between the first five layers and the associated change in surface energy ($\Delta\sigma$) for three different DFT functionals: the LDA, the BLYP-GGA functional used throughout this work, and the "simple" GGA functional of Perdew, Burke, and Ernzerhof[94] (PBE). Comparison is also made to earlier LDA,[48,53,55] Perdew-Wang[95] (PW) and BLYP GGA[55,54] and Hartree−Fock (HF) predictions,[52] and to values determined from X-ray[36] and ion scattering[20] experiments. Because the various calculations differ in many computational details (e.g., the number of O layers considered, which are listed explicitly in Table 1, as well as basis sets, lateral supercell size, ***k*** point sampling, and other factors), comparisons must be made with care.

In general, the DFT results for the relaxed geometry and relaxation energy are reasonably consistent. The largest deviations occur for the PBE functional and for the BLYP calculations of ref 54 (which used a 40 Ry planewave cutoff that was probably too small). There is no significant difference even between the LDA and GGA, nor between calculations for different slab thicknesses; extensions beyond three O layers[53,55] tend only to affect deeper layer spacings, and only by ∼10% at most. The HF results in Table 1 also agree reasonably well with the DFT predictions for deeper layers, but yield a ∼25% larger relaxation energy and a reduction in the outermost Al−O separation of only 68% instead of 80−90% in DFT. (Earlier HF calculations,[43] based on more limited basis sets, predicted reductions as small as 48%.) The qualitative relaxation pattern predicted by both DFT and HF is consistent with available experimental data,[20,36] but significant quantitative discrepancies exist for each of the first three layer spacings. It would be extremely surprising if the relatively low values inferred from experiments for the outer Al layer relaxation (51 and 63%) reflected an inherent failure of DFT and/or superiority of HF for this system. Instead, we suspect that most of this disagreement is due to difficulties in surface preparation; even with annealing temperatures of 1100 °C, Ahn and Rabalais[20] observed significant amounts of surface H during their measurements ([H]/[Al] ≈ 1/3), which the results below indicate would cause dramatic changes in surface geometries.

Within the BLYP-GGA, the relaxation of surface Al is accompanied by a 9% reduction in the length of bonds to second-layer O (to 1.687 Å). Again, the experimentally derived value[36] for this reduction (4.5 ± 2.5%) is smaller than predicted, but in neither case would we characterize the relaxation as bond-length conserving.[36,49] The reduction is a natural consequence of the reduced coordination of surface Al. Undercoordination of the outermost O atoms also causes a shortening of bonds to interior Al neighbors, to 1.804 Å (−3%) and 1.889 Å (−4%). These reductions result in part from small lateral displacements within the O layer, which manifest themselves primarily as slight disortions and rotations of the triangles of O atoms below each surface Al. The predicted lateral displacement pattern agrees qualitatively with that determined experimentally.[36]

The low coordination of surface Al atoms on clean α-Al_2O_3 (0001) makes these sites strong Lewis acids (electron acceptors) which readily adsorb H_2O molecules through their O atoms (O_{ads}). In the extremely low coverage regime of one H_2O molecule per supercell (or 0.57 H_2O per nm^2), we find that H_2O prefers to dissociate, but can also adsorb in a metastable molecular binding mode (Figure 2a). Molecular adsorption occurs through a dative bond between surface Al and O_{ads} that binds H_2O by 23.3 kcal mol^{-1} (Table 2). Dissociative adsorption is 7−10 kcal mol^{-1} more favorable and is primarily heterolytic in nature: i.e., adsorbed H_2O can be viewed as splitting into H^+ and OH^-, with the proton transferred to a nearby surface O (O_s). A "1−2" dissociated state in which O_s is a nearest neighbor of the Al to which O_{ads} binds (Figure 2b) is lowest in energy, followed closely by a "1−4" dissociated state in which O_s is across a 6-fold ring from this Al (Figure 2c). A more distant separation between O_s and O_{ads} (e.g., "1−6" dissociation, Figure 2d) is less favorable than either of these states by over 2 kcal mol^{-1}.

In all cases, adsorption of H_2O significantly disrupts the clean α-Al_2O_3 (0001) surface geometry. Optimized bond lengths and Al distances above the outermost O plane are given in Figure 2 and Table 2 for the four binding modes considered. Molecular adsorption produces a relatively long Al−O_{ads} bond (1.953 Å) that pulls the surface Al out to −49% (from −82%) of its bulk distance to second-layer O and elongates its three other bonds to neighboring O by nearly 2%. The Al−O_{ads} bond is much shorter in the three dissociated states, and the Al is pulled out much further, nearly to its bulk position. Bonds between this Al and second-layer O are significantly longer than in the molecularly adsorbed state, and Al−O_s bonds are elongated even beyond bulk values.

Still more remarkable is a dramatic adsorbate-induced restructuring[96] in the vicinity of the O_s sites in the 1−4 and 1−6 geometries. In both cases, as can be seen in the side views in Figures 2c and 2d, the "surface" Al bound to O_s descends below the outermost O layer to the depth of third-layer Al and becomes effectively 6-fold coordinated. This effect is clearly a response to the large change in electrostatic potential that

TABLE 1: Comparisons of Predicted (based on slab models with different numbers of O layers) and Observed Relaxations of the Outermost Interlayer Spacings (in %) and Changes in Surface Energy upon Relaxation ($\Delta\sigma_{rel}$, in Jm^{-2}) for a Clean α-Al_2O_3 (0001) Surface

	this work[a]			previous calculations[b]								expt.	
	LDA	BLYP	PBE	LDA	LDA	LDA	LDA	LDA	PW	BLYP	HF		
ref				48[c]	53[d]	53[d]	53[d]	55[e]	55[f]	54[g]	52[h]	36	20
# O layers	3	3	3	3	3	9	18	9	9	7	3		
$Al_1 - O_2$	−92	−82	−98	−86	−86	−86	−87	−86	−85	−70	−68	−51	−63
$O_2 - Al_3$	+4	+7	+5	+3	+3	+3	+3	+3	+3	+10	−1	+16	−
$Al_3 - Al_4$	−51	−49	−48	−54	−54	−42	−42	−44	−45	−34	−45	−29	−
$Al_4 - O_5$	+24	+25	+21	+25	+25	+18	+19	+20	+20	+19	+22	+20	−
$\Delta\sigma_{rel}$	−1.98	−1.89		−2.01				−2.02	−1.99	−3.1	−2.56		

[a] Based on 3 × 3 surface cell and other computational details in text. [b] Based on 1 × 1 surface cells and varying numbers of *k* points (not always specified). [c] Norm-conserving pseudopotentials (NCPP), 46 Ry planewave cutoff (PWC). [d] NCPP, Gaussian DZP basis. [e] NCPP, ∼66 Ry PWC. [f] Ultrasoft pseudopotentials, ∼44 Ry PWC. [g] NCPP, 40 Ry PWC. [h] Basis: 85−11G for Al, 8−411G for O.

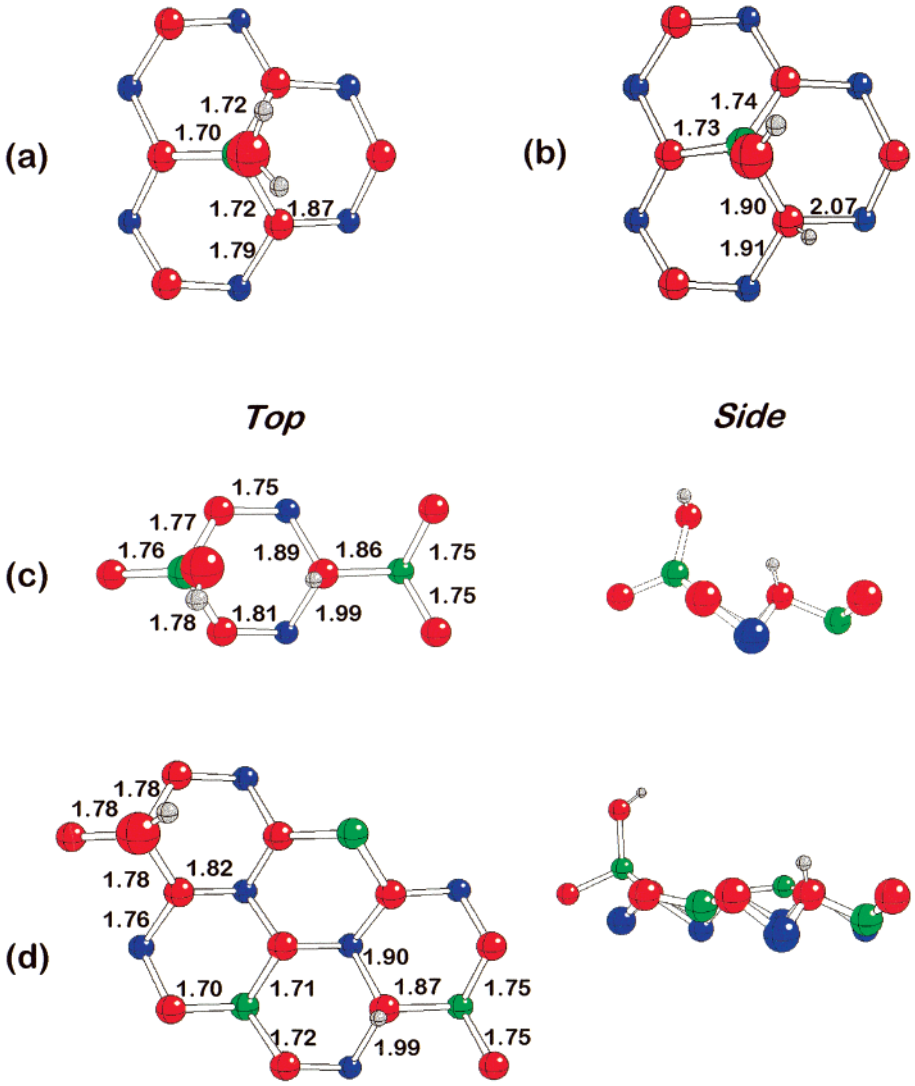

Figure 2. Selected portions of optimized supercells with single H_2O adsorbed molecularly (a) and dissociatively in 1−2 (b), 1−4 (c), and "1−6" (d) geometries. Top and side views are shown for (c) and (d) to emphasize descent of some surface Al below outermost O layer. Atoms are color coded as in Figure 1, with smaller gray spheres added to represent H. Selected Al−O bond lengths are given in Å.

accompanies the addition of a proton to O_s. In the case of 1−6 dissociation, the surface Al across a 6-fold ring from O_s also descends slightly below the outermost O layer (by ∼0.3 Å), but not to the point of increasing its effective coordination. The prediction of these complex structural changes that accompany H_2O dissociation is only possible in the present work because of the large supercells employed, which allow relaxation effects to extend over a wide range, both laterally and into the surface.

Molecular adsorption of H_2O leaves the two O_{ads}−H bonds roughly the same length as in an isolated molecule (calculated to be 0.973 Å). Dissociation on clean α-Al_2O_3 (0001), on the other hand, produces two distinct types of hydroxyl group: O_s−H, with a bond length similar to that in the molecule or molecularly adsorbed state, and O_{ads}−H, which is shorter by over 1%. This difference is a consequence of the higher coordination of O_s compared to O_{ads}, which we will see in section 4C, also manifests itself in a difference in O−H vibrational frequencies.[10,11,16−19] The present finding that in all

TABLE 2: Low-Coverage Supercell Results for Binding Energies and Selected Geometric Parameters for Various States of H_2O Adsorption on α-Al_2O_3 (0001)

	molecular	1−2 dissoc.	1−4 dissoc.	1−6 dissoc.
binding energy[a]	23.3	33.2	32.5	30.4
$H-O_{ads}$[b]	0.978, 0.978	0.966	0.967	0.966
$H-O_s$[b]		0.978	0.974	0.973
O_{ads}-Al[b]	1.953	1.727	1.739	1.736
$Al-O_{plane}$[c]	0.43	0.73	0.72	0.74
	(−49%)	(−13%)	(−14%)	(−12%)

[a] In kcal mol^{-1}. [b] In Å. [c] Average height of Al bound to O_{ads} above second-layer O atoms, in Å, with percent relaxation relative to bulk interlayer spacing in parentheses.

dissociated states the transferred proton associates itself with a specific O_s site, as opposed to lying near the center of the hollow region between neighboring O_s sites, is consistent with chemical intuition, but is not always correctly described by classical force fields.[47b]

The binding energies for dissociative H_2O adsorption in Table 2 are within the range of experimental values (23 to 41 kcal mol^{-1}) extracted from H_2O desorption measurements[15b] on carefully prepared α-Al_2O_3 (0001). Most earlier experiments[21−25,29,30] gave values near or above the upper end of this range, but as will be discussed further in section 4B, quantitative comparisons are complicated by variations in binding energy due to surface coverage and defects, which are difficult to characterize adequately.

That a relatively isolated H_2O molecule prefers to adsorb dissociatively on α-Al_2O_3 (0001), even in the absence of defects, differs from the behavior predicted in an earlier CPMD study[66] of H_2O on MgO (100). In that case, dissociative adsorption was favored in the vicinity of a step, but molecular adsorption was more stable on the ideal surface. The predicted metastability of molecularly adsorbed H_2O on α-Al_2O_3 (0001) also differs from earlier small-supercell DFT results for H_2O on TiO_2 (110) and SnO_2 (110), which found only dissociative adsorption at low coverages.[71a] The stabilities of different H_2O binding modes on different metal-oxide surfaces clearly depend on such factors as the surface structure, acidity of the surface metal site, and basicity of surface O. Dissociative adsorption is more favorable on α-Al_2O_3 (0001) than MgO (100), for example, because 3-coordinated surface Al is a much stronger Lewis acid than 5-coordinated surface Mg. Static equilibrium calculations for low H_2O coverages on ideal surfaces, of course, are only a first step toward understanding the full effects of hydration. One also needs to consider the dynamics of various processes,[60,66,71b] the effects of interactions between H_2O molecules,[60,69,70,71c,72] the roles of defects[66] and varying pH,[58] and the possibility of massive reorganizations involving the transport of surface ions.[4,67]

B. Cluster Calculations. Before considering any of these complications, we briefly contrast the above supercell results with analogous cluster-model calculations. Prior to the present work, the only quantum-chemical calculations that have addressed the issues of H_2O adsorption and dissociation on α-Al_2O_3 (0001) modeled the surface with small clusters containing 3-coordinated Al sites.[46,57,58] Of particular interest, for the purpose of comparison, are the recent HF and hybrid-DFT (B3LYP functional[97]) calculations of Wittbrodt, Hase, and Schlegel[57] for clusters as large as Al_8O_{12}. To separate the effects of model differences from those of the different methodologies and basis sets employed, we have repeated many of the cluster calculations in ref 57 with the same CPMD formalism and BLYP-GGA functional used in section 3A. As in ref 57, we constrain most of the cluster atoms to the positions they would have in a bulk crystal in order to avoid any unphysical relaxations that might result from the finite lateral extent of the cluster.

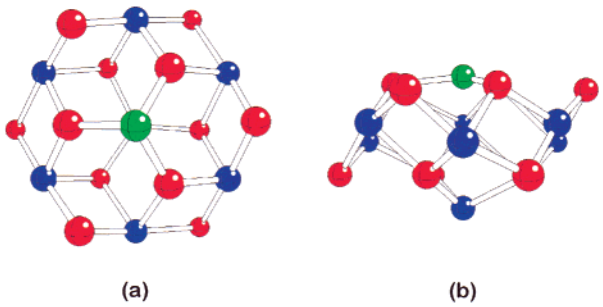

Figure 3. Top (a) and side (b) views of relaxed Al_8O_{12} cluster model used to represent clean α-Al_2O_3 (0001). Colors same as in Figure 1. Only the surface Al (green) and neighboring three O atoms are unconstrained.

TABLE 3: Al_8O_{12} Cluster Model Results for Binding Energies and Selected Geometric Parameters for Various States of H_2O Adsorption

	molecular	1−2 dissoc.	1−2 rebonded
binding energy[a]	25.7	28.9	46.5
$H-O_{ads}$[b]	0.979, 0.979	0.970	0.967
$H-O_s$[b]		0.981	0.971
O_{ads}-Al[b]	1.953	1.723	1.706
$Al-O_{plane}$[c]	−49%	−13%	+11%

[a] In kcal mol^{-1}. [b] In Å. [c] Average height of Al bound to O_{ads} above second-layer O atoms, relative to unrelaxed (bulk) value.

A clean α-Al_2O_3 (0001) surface is modeled in this approach by the partially relaxed, neutral Al_8O_{12} cluster in Figure 3. Only the surface Al atom (green) and its three nearest O neighbors are unconstrained. Relaxation reduces the height of this Al above the average height of second-layer O by 66%, in qualitative agreement with ref 57 and with the above supercell results. At the same time, the three unconstrained O atoms in the second layer move slightly outward (by 0.12 Å), and their bonds to surface Al shrink by 5% (to 1.754 Å). These structural changes lower the energy of the cluster by 41.9 kcal mol^{-1}, which translates into a decrease in surface energy of 1.49 J/m^2. This value is in good agreement with the B3LYP results of ref 57 but is 21% less than the BLYP supercell prediction in Table 1.

Of the possible H_2O binding modes on α-Al_2O_3 (0001), the Al_8O_{12} cluster model is most successful in reproducing the supercell predictions for the most weakly bound, molecular state. The calculated cluster adsorption geometry in this case is similar to that in Figure 2a, and the specific distances listed in Table 3 are in excellent agreement with those in Table 2. Interlayer Al−O bonds are about 5% longer in the cluster than in Figure 2a, and the H_2O binding energy is slightly larger (by 2.4 kcal mol^{-1}). The predicted binding energy of 25.7 kcal mol^{-1} is 5.9 kcal mol^{-1} less than the B3LYP/6-31+G* prediction for H_2O binding to Al_8O_{12}, which is itself below the HF/6-31+G* prediction.[57]

Attempts to optimize a 1−2 dissociated state for H_2O on an Al_8O_{12} cluster yield two distinctly different results, depending upon the starting configuration. One of the minima has a geometry very similar to the supercell result in Figure 2a, with the exception that the bond between surface Al and O_s is considerably longer in the cluster model (2.25 Å). Table 3 indicates that the H_2O binding energy for this state is 28.9 kcal mol^{-1}, 4.3 kcal mol^{-1} lower than the supercell result in Table 2. This underestimate of the energy for dissociative adsorption in the cluster model, as well as the larger magnitude of the discrepancy compared to that for molecular adsorption, is

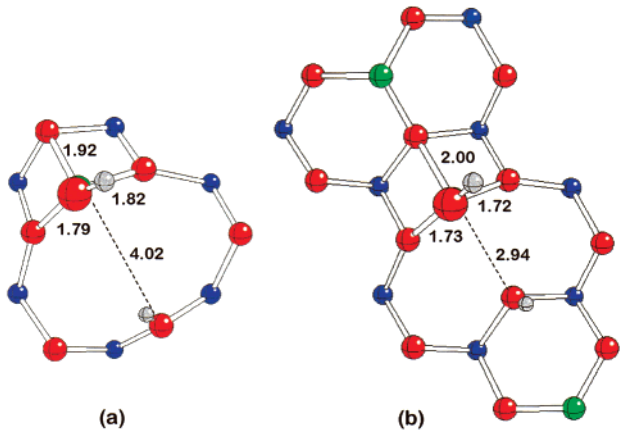

Figure 4. Selected portions of relaxed cluster (a) and supercell (b) models for H_2O adsorbed in "rebonded" 1−2 dissociated state. Colors same as in Figure 2. Distances from surface O to Al atoms bound to O_{ads} indicated in Å.

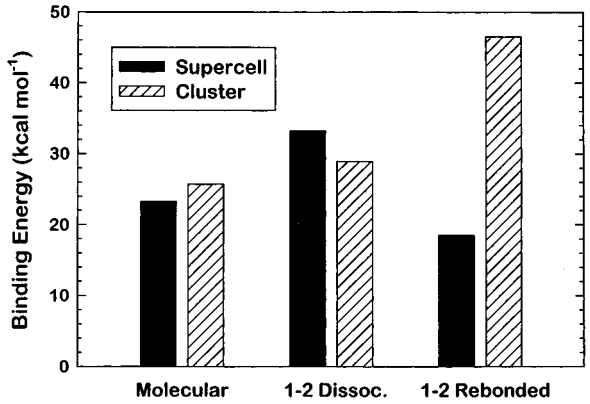

Figure 5. Comparison of supercell and cluster model predictions for H_2O binding energies in different adsorption states.

consistent with an earlier comparison[98] made for H_2O adsorption on MgO. The dissociated state involves stronger electrostatic interactions, which are more sensitive to the long-range environment. Dissociation into the 1−2 state analogous to that in Figure 2a remains favored over molecular adsorption in the cluster model, but by only 3.2 kcal mol^{-1}, as opposed to 9.9 kcal mol^{-1} in the supercell. The B3LYP/6-31+G* cluster results in ref 57 predict an even smaller preference for this type of dissociation.

The second minimum that exists for 1−2 dissociation within the Al_8O_{12} cluster model is much lower in energy and involves a significant lateral displacement and rebonding of the surface Al atom. As can be seen in Figure 4a, the bond between this Al and O_s is broken (stretched to 4.02 Å), while a new bond forms to a second-layer O on the periphery of the cluster. The H_2O binding energy for this state is 46.5 kcal mol^{-1} (Table 3), roughly 20 kcal mol^{-1} greater than that for either molecular adsorption or unreconstructed 1−2 dissociation. With some effort, we were able to locate an analogous 1−2 rebonded state in the supercell model. The optimized structure (Figure 4b) differs primarily from that in the cluster model by having a much shorter Al−O_s distance (2.94 Å) because of steric constraints that prevent O_s from relaxing as far laterally. The resulting H_2O binding energy in the supercell model is only 18.5 kcal mol^{-1}. A graphical comparison of binding energies in Figure 5 shows that this 1−2 rebonded state is less stable even than molecular adsorption in the supercell model, but is artificially stabilized by a large amount in the cluster model. The overall preference for a 1−2 rebonded state on an Al_8O_{12} cluster was not considered in ref 57, although similar rebonding effects were predicted in that work for the dissociative adsorption of two or three H_2O molecules near the same Al site. While we have not attempted to compare supercell and cluster results for systems with more than one H_2O molecule, the large discrepancy in Figure 5 for the 1−2 rebonded state raises concerns about the validity of any cluster model prediction that involves large relaxations near the periphery.

Wittbrodt, Hase, and Schlegel[57] also examined 1−4 dissociation on an Al_8O_{12} cluster, with O_s free to move except for one remaining constraint on one of its dihedral angles with interior atoms. At all levels of theory, they found 1−4 dissociation to be 3−4 kcal mol^{-1} *less* favorable than molecular H_2O adsorption. This is in sharp disagreement with the supercell results in Table 2, which predict 1−4 dissociation to have a comparable binding energy to 1−2 dissociation and to be favored over molecular adsorption by 9.2 kcal mol^{-1}. This discrepancy is not surprising, given that (1) the O_s proton acceptor is undercoordinated compared to a real α-Al_2O_3 (0001) surface, (2) an Al_8O_{12} cluster lacks the neighboring surface Al that was found to relax into the surface in the 1−4 supercell state (Figure 2c), and (3) such a small cluster was shown above to be inadequate even for 1−2 dissociation, where edge effects should be less important. Because of these obvious limitations, we do not even attempt to examine 1−4 dissociation on Al_8O_{12} clusters within the present formalism. We also do not consider the issue of barriers to H_2O dissociation on such clusters, except to point out that the values predicted in ref 57 for 1−2 and 1−4 dissociation (9.3 and 14.8 kcal mol^{-1}, respectively, for the most accurate B3LYP calculations) are distinctly different from the supercell predictions that follow in section 3C.

While it is dangerous to generalize on the basis of the present limited analysis, it is clear that one must be extremely careful when attempting to model the chemistry of extended metal−oxide surfaces using finite clusters.[99] How much larger a cluster than Al_8O_{12} and/or what type of embedding procedure one needs to consider in order to achieve accuracies comparable to supercell calculations for ideal α-Al_2O_3 (0001) remains to be seen. Small cluster models may nevertheless be useful for rapidly identifying possible trends, binding modes, and reactions,[100] and for gaining qualitative insights into behaviors on nonideal surfaces. The significantly larger H_2O binding energy predicted here for the 1−2 rebonded state on Al_8O_{12}, for example, suggests a preference for H_2O binding (and dissociation) in the vicinity of surface defects (e.g., a step), where large relaxations and rebonding are more favorable because of reduced coordinations and steric effects. Such a preference is consistent with experimental evidence for enhanced heats of adsorption at very low H_2O coverages,[21−25,29,30] an issue to which we will return in section 4B.

C. Constrained Dynamical Calculations of Dissociation Barriers. The static supercell calculations in section 3A predict a slight thermodynamic preference for 1−2 over 1−4 dissociation at low coverages. While it would be desirable to examine the dynamics of these reactions directly with CPMD, such an approach is impractical for all but the fastest chemical reactions because crossings through transition states (i.e., over energy barriers) generally occur too rarely on typical simulation time scales. We therefore adopt the constrained dynamics approach of refs 89−91 and calculate free-energy profiles along both types of dissociation pathways from the common starting point of molecularly adsorbed H_2O. The reaction coordinate for each pathway is the distance between the transferring proton and the O_s site to which it transfers. This coordinate was constrained to values between those in the molecularly adsorbed initial states

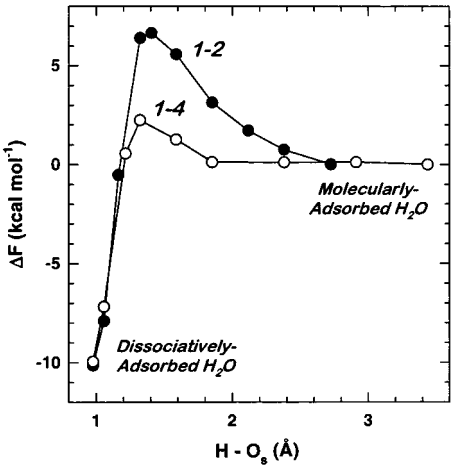

Figure 6. Constrained-dynamics predictions of free energy changes at 300 K along pathways for 1−2 and 1−4 dissociation of single H_2O molecule per supercell. Reaction coordinate is distance between transferring proton and relevant O_s site. Reference free energy is value in molecularly adsorbed state. Estimated statistical errors are ± 1 kcal mol^{-1}.

(> 2.7 Å) and 0.97 Å in the dissociated states, with the typical step size being 0.5 au (0.26 Å). For each H−O_s distance considered, the average constraint force was calculated at 300 K from a temperature-controlled[87,90,91] dynamics run of at least 0.2 ps after an initial equilibration period. The final configuration for one run was used as the starting configuration for the next value of the constraint. Each equilibration period was long enough to ensure a stable average. Larger fluctuations in the instantaneous constraint force were observed at intermediate H−O_s distances, and longer run times were required in some of these cases to avoid errors due to trapping in local minima (e.g., the transferring proton temporarily forming hydrogen bonds to O_{ads} or to surface oxygen other than O_s).

Integration of the average constraint forces along the reaction coordinates yields the variations in free energies for 1−2 and 1−4 dissociation at 300 K shown in Figure 6. Both types of dissociation are predicted to be exothermic by ∼10 kcal mol^{-1}, which is close to the values 9.9 and 9.2 kcal mol^{-1}, respectively, obtained from the binding energy differences in Table 2. This agreement provides an important consistency check, as entropic contributions to the free energy differences between molecularly adsorbed and dissociatively adsorbed states of H_2O are estimated to be small at 300 K. The numerical accuracy of the reaction free energies obtained from Figure 6 is on the order of ±1 kcal mol^{-1}, given the statistical variations in our calculated constraint forces. While the nearly equal thermodynamic driving forces predicted for 1−2 and 1−4 dissociation may be largely fortuitous, the greater similarity in predictions based on ΔF values compared to those based on binding energy differences is consistent with our qualitative expectation that the 1−4 dissociated state has a slightly higher vibrational entropy than the 1−2 state.

In addition to providing thermodynamic information, Figure 6 allows us to compare the rates of 1−2 and 1−4 dissociation at 300 K. The calculated free-energy barrier ($\Delta F^{\ddagger}$) that must be overcome, beginning with molecularly adsorbed H_2O, is three times larger for the 1−2 reaction: 6.6, vs 2.2 kcal mol^{-1} for the 1−4. Reaction rates (k) follow from the transition-state theory expression

$$k = (k_B T/h)e^{-\Delta F^{\ddagger}/k_B T} \qquad (1)$$

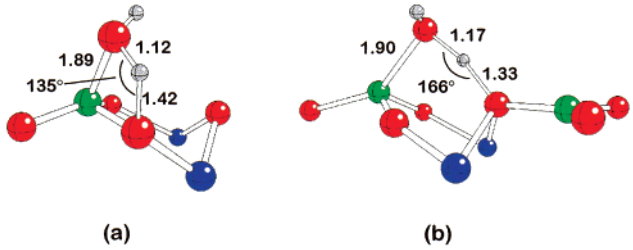

Figure 7. Selected portions of approximate transition state geometries for 1−2 (a) and 1−4 (b) dissociation of a single H_2O molecule in a supercell. Colors same as in Figure 2. Distances in Å.

where k_B and h are Boltzmann's and Planck's constants, respectively. For 1−4 dissociation at 300 K, eq 1 yields $k \approx 1.6 \times 10^{11}$ s^{-1}, which is more than 3 orders of magnitude larger than the result $k \approx 10^8$ s^{-1} for 1−2 dissociation. (The above statistical errors alone introduce uncertainties in these absolute rate constants of close to an order of magnitude; other potential sources of error are more difficult to quantify.) The 1−4 channel obviously dominates and yields a half-life for isolated, molecularly adsorbed H_2O on otherwise clean α-Al_2O_3 (0001) of $\tau_{1/2} = \ln 2/k \approx 4.3$ ps. On the time scale of a typical CPMD simulation, observation of a spontaneous 1−4 dissociation event may thus be barely possible, while observation of a spontaneous 1−2 event is highly unlikely. On more macroscopic time scales, all adsorbed H_2O at low coverages would be dissociated. In fact, given that the energy released upon molecular adsorption is much greater than the barrier to either 1−4 or 1−2 dissociation, it is likely that an isolated gas-phase molecule impinging on α-Al_2O_3 (0001) would go directly into a dissociated state, instead of equilibrating temporarily in a molecularly adsorbed state.

The different barriers for 1−2 and 1−4 dissociation reflect the different transition states in the two reactions. Figure 7 shows approximate geometries for these transition states, obtained by loose energy minimizations with the H−O_s bonds constrained to the values for which the curves in Figure 6 peak. The most significant differences between the 1−2 (Figure 7a) and 1−4 (Figure 7b) results are that the O_{ads}−H−O_s linkage in the former is severely bent (∼135°) and part of a four-membered ring, while in the latter it is more nearly linear and part of a six-membered ring. Qualitatively, these structures are similar to those obtained by averaging the coordinates in the 300 K dynamical trajectories with the same H−O_s constraint[60] and to the transition states in ref 57; the latter cluster calculations, of course, omit the surface Al bound to O_s, which is partially descended in Figure 7b below the outermost O layer (a consequence of its subsurface nature upon complete 1−4 dissociation). While we have not attempted to obtain accurate barrier heights at any other temperature, the constrained minimizations that led to Figure 7 suggest that the difference between the 300 K $\Delta F^{\ddagger}$ values for 1−2 and 1−4 dissociation is largely energetic in nature, but is enhanced further by entropy. It is well known from previous computational studies that barrier heights for X−H→Y proton-transfer reactions increase with the angle between X−H and H−Y bonds.[101] Entropic contributions also favor the 1−4 reaction because its 6-fold ring transition state is considerably more floppy than the 4-fold ring in the 1−2 case.

We expect that the main qualitative conclusion of this section—that 1−4 dissociation is strongly favored kinetically over 1−2 dissociation—is robust. Nevertheless, significant quantitative uncertainties remain because of our neglect of nuclear quantum effects[86] and the uncertain accuracy of GGA energy barriers for proton-transfer reactions.[102]

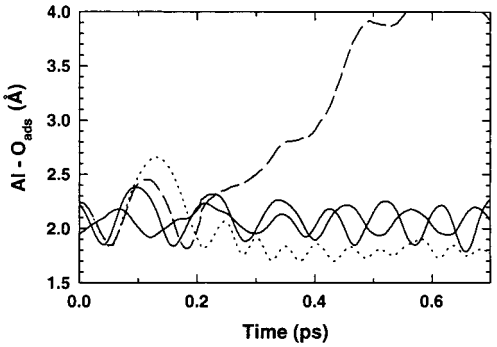

Figure 8. Time dependence of selected Al−O_{ads} bond lengths during dynamical simulation begun with nine molecularly adsorbed H_2O per supercell (one for each surface Al). Solid curves are typical behavior. Dashed curve corresponds to molecule that breaks chemisorption bond at ∼0.3 ps. Dotted curve corresponds to molecule that undergoes unimolecular 1−4 dissociation at ∼ 0.24 ps.

4. Intermediate H_2O Coverages

A. Unconstrained Dynamical Simulations. We began our study of higher H_2O coverages by performing a number of unconstrained dynamical simulations with nine H_2O molecules either preadsorbed or near one surface in our 3 × 3 supercell model. The most informative of these simulations was initiated with each H_2O in a randomly oriented state of molecular adsorption to one of the nine surface Al sites. No temperature controls were imposed, but energy was gradually added until the system first equilibrated near 250 K for ∼0.7 ps and then near 350 K for an additional 0.3 ps. The molecules were initially too far apart to form direct bonds, but they could sense each other's presence through their interactions with the surface and through long-ranged dipole-dipole interactions. Most molecules remained molecularly adsorbed throughout the simulation, but a few exhibited more chemically significant behavior.

Figure 8 shows the temporal evolution of some Al−O_{ads} distances while the system temperature was ≤ 250 K. The solid curves show typical oscillations for molecules that remain intact and chemisorbed. The frequencies of these vibrations are < 400 cm^{-1}, which places them within the range of bulk lattice modes[103] (<750 cm^{-1}). The dotted curve corresponds to a molecule that spontaneously dissociated at ∼0.24 ps, as will be discussed further below. Consistent with the optimized geometries in Table 2, the average Al−O_{ads} bond length after dissociation is over 0.2 Å less than in molecularly adsorbed H_2O. The dashed curve in Figure 8 corresponds to a different molecule that broke its bond to surface Al in an event that was nearly concurrent with, but independent of, the spontaneous dissociation. This molecule remained physisorbed on the surface for the duration of the simulation, but diffused laterally away from and never returned to its original Al site. As it diffused, it temporarily formed a hydrogen bond to a neighboring adsorbed H_2O and subsequently moved on to facilitate the dissociation of yet another adsorbed H_2O (vide infra). The mobile physisorbed state of this molecule may be viewed as a precursor to chemisorption in that it results from a relatively weak attraction to the surface in general, as opposed to a specific adsorption site. (For H_2O on alumina, this attraction remains primarily electrostatic, with dispersion forces playing a negligible role.) The concept of a mobile precursor state has long been postulated in the surface science literature, but has only recently been confirmed experimentally.[104]

Details of the first, *unimolecular* dissociation event are provided in Figure 9. This reaction occurs via a 1−4 pathway, as shown schematically in the inset. The transferring proton (H_t)

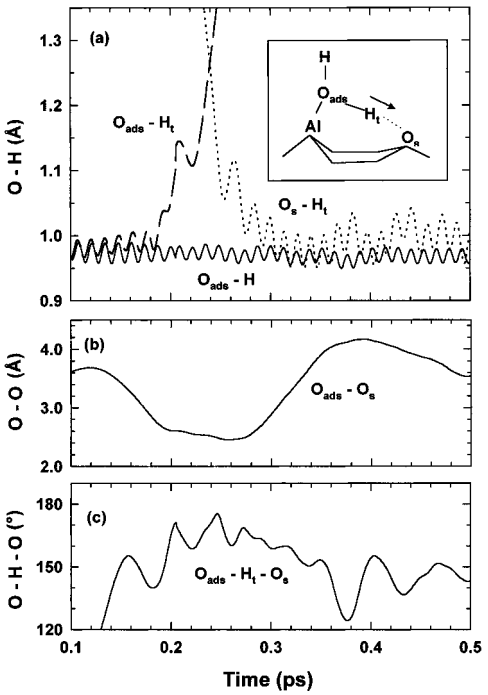

Figure 9. Time dependence of selected O−H (a) and O−O distances (b) and O−H−O angle (c) associated with spontaneous unimolecular 1−4 dissociation reaction observed during same dynamical simulation as Figure 8. Inset to (a) shows schematic geometry in vicinity of reaction, with arrow showing the direction of proton transfer.

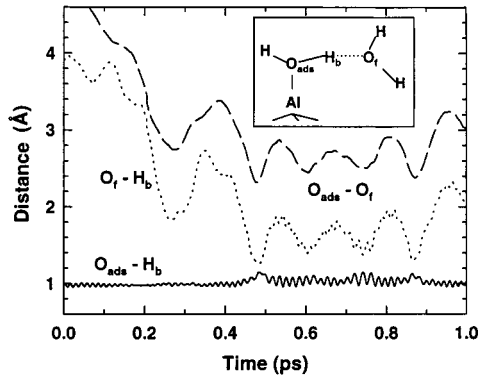

Figure 10. Time dependence of selected interatomic distances associated with temporary formation of H bond between one molecularly adsorbed H_2O and one "free" H_2O during same dynamical simulation as Figure 8. Inset shows schematic geometry in vicinity of H bond.

shifts very rapidly along a hydrogen bond between the water oxygen to which it is initially bound and the relevant O_s site. The entire process of breaking the O_{ads}−H_t bond and forming the O_s−H_t bond takes only 0.12 ps. The transfer is facilitated by a dramatic reduction in O_{ads}−O_s distance during that time period (to < 2.6 Å) and an increase in the O_{ads}−H_t−O_s angle to nearly 180°. The energy released upon dissociation causes the O_s−H_t bond to remain vibrationally excited long after the transfer, as evidenced by the large amplitude of its oscillations. As expected from static calculations, the average O_s−H_t and residual O_{ads}−H distances after dissociation are, respectively, longer and shorter than that of the initial water O−H bonds.

Interatomic distances associated with the temporary intermolecular hydrogen bond that forms near a different surface Al site are plotted in Figure 10. The oxygen of the "free" H_2O molecule (O_f) is pulled toward one of the hydrogens (H_b) associated with a neighboring molecularly adsorbed H_2O from ∼0.5 to ∼0.9 ps. During that time, the average O_{ads}−O_f and

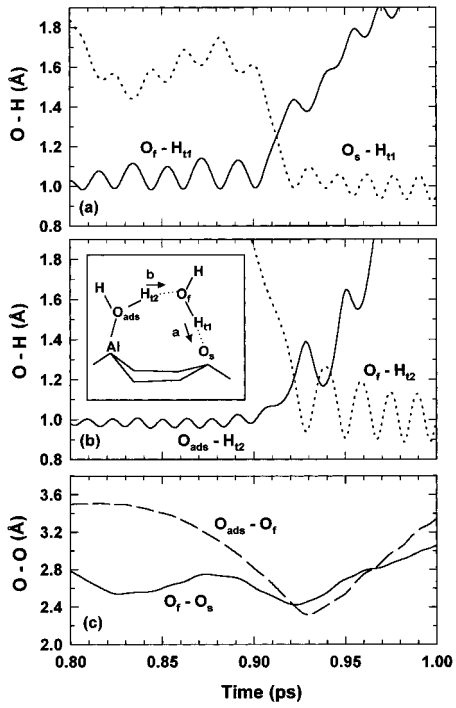

Figure 11. Time dependence of selected O−H (a,b) and O−O (c) distances associated with H_2O-catalyzed 1−4 dissociation reaction observed during same dynamical simulation as Figure 8. Inset to (b) shows schematic geometry in vicinity of reaction, with arrows showing directions and sequence of proton transfers.

O_f−H_b distances are reduced to 2.6 and 1.6 Å, respectively, and the average O_{ads}−H_b distance is slightly elongated. As discussed extensively in ref 66(b), the frequency of O_{ads}−H_b vibrations is strongly red shifted and homogeneously broadened by hydrogen bonding; the latter effect is a consequence of the light H atom effectively responding instantaneously to the much slower oscillations in the O_{ads}−O_f distance. The amplitude of O_{ads}−H_b vibrations is also enhanced by the initial contact with free H_2O. The breaking of the hydrogen bond near 0.9 ps occurs shortly after, and is most likely precipitated by, the increase in temperature to ∼350 K.

A second, unanticipated, type of dissociation reaction occurs almost immediately after the free H_2O molecule moves on toward a different molecularly adsorbed H_2O. The free molecule facilitates a 1−4 dissociation of the adsorbed molecule via a synchronous transfer of two protons.[57,60] Details of this event are provided in Figure 11, with the relevant geometry sketched in the inset; the transfers of the first (H_{t1}) and second (H_{t2}) protons are separated in panels (a) and (b) for clarity. The reaction is preceded by the formation of a hydrogen bond between the free H_2O and the O_s site. This is apparent from the relatively short O_s−H_{t1} and O_f−O_s distances for the first 0.1 ps in panels (a) and (c), respectively. The formation of this bond causes the O_f−H_{t1} bond length in the "free" molecule to elongate (from an average value of 0.97 Å) and to become highly excited vibrationally. While this molecule is bound to the O_s site, it reorients itself and forms a second hydrogen bond to the preadsorbed molecule, similar to that in Figure 10. This bonding causes the O_f−H_{t2} and O_{ads}−O_f distances in panels (b) and (c) to decrease rapidly near 0.9 ps and sets up the concerted reaction. The O_f−H_{t1} and O_s−H_{t1} curves in (a) cross at ∼0.91 ps, and the O_{ads}−H_{t2} and O_f−H_{t2} curves in (b) begin crossing only 10 fs later. The second proton transfer takes two vibrational periods to complete (the curves in (b) cross back temporarily at 0.94 ps), but the entire reaction is completed in <50 fs. After the reaction, the O_f−H_{t2} bond in the newly formed "free" H_2O molecule remains highly excited, and there is no evidence in (c) of prolonged residual hydrogen bonding. The new O_f-containing water molecule simply moves on to another part of the surface, containing one different proton than it had initially and leaving a 1−4 dissociated H_2O in its wake.

H_2O-mediated reactions of this type have been studied extensively in many other contexts,[105−110] but the present work is, to our knowledge, the first in which such a reaction was observed to occur spontaneously in a first-principles dynamical simulation. That the two proton transfers in Figure 11 are essentially synchronous, as opposed to stepwise, is particularly noteworthy and consistent with expectations for multiple hydrogen bonds within a closed topological loop.[101] We have not attempted to determine whether free H_2O actually catalyzes 1−4 dissociation, but the fact that the H_2O-mediated reaction exploits the only opportunity it has in the above simulation suggests that its rate is at least comparable to that of unimolecular 1−4 dissociation. This and other multiple proton transfer reactions are likely to increase in importance at higher H_2O coverages, where the probability of formation of multiple hydrogen-bonded configurations is much higher.

Although interesting, a single simulation of this kind has little statistical significance. Nevertheless, it is reassuring that the one and only one unimolecular 1−4 dissociation event observed for nine preadsorbed H_2O molecules in ∼1 ps of dynamics is exactly what one would expect from the rate for this process calculated from Figure 6. This consistency implies that the dynamics of unimolecular dissociation are not strongly dependent on H_2O coverage, at least between 0.6 and 5.1 H_2O per nm^2. That we do not observe any 1−2 dissociation events, despite many near approaches to the transition-state geometry in Figure 7a, is also consistent with the orders-of-magnitude lower rate predicted for this pathway in section 3C.

Other simulations performed for the same coverage of H_2O, but different starting configurations, were generally less informative. Most of these were begun with one H_2O already in a 1−4 dissociated state and eight others either molecularly adsorbed on neighboring Al sites or in a second H_2O layer. Molecules not in direct contact with the surface tended to form intermolecular hydrogen bonds, as in H_2O droplets, which prevented their local configurations from evolving much further.

The only additional reaction that was observed involved the transfer of a proton at ∼300 K from one molecularly adsorbed H_2O to the residual O_{ads}−H group associated with the predissociated molecule. Details are provided in Figure 12, with the schematic geometry inset. The transfer occurs at ∼0.26 ps, after a long period in which the hydroxyl group oxygen (O_{ads}-(1)) attracts the relevant proton (H_t) and water oxygen (O_{ads}-(2)) through a nearly linear hydrogen bond. Upon forming the new $O_{ads}(1)$−H_t and breaking the $O_{ads}(2)$−H_t bonds, the Al−$O_{ads}(1)$ and Al−$O_{ads}(2)$ distances interchange (as expected from Table 2) and the hydrogen bond linking $O_{ads}(1)$ and $O_{ads}(2)$ breaks. The overall reaction is thermoneutral, and its spontaneous occurrence implies a small or vanishing energy barrier. The net effect of interchanging Al−OH and Al−OH_2 sites provides a general mechanism by which protons may diffuse on partially hydroxylated alumina surfaces. This mechanism may be responsible in part for the dynamical behavior invoked by Huggins and Ellis[111] to account for the observed temperature dependence of alumina ^{27}Al nuclear magnetic resonance spectra.

B. Coverage Dependence of Binding Energies. Selected geometry optimizations with more than one H_2O molecule per supercell indicate that (1) binding energies for both molecular

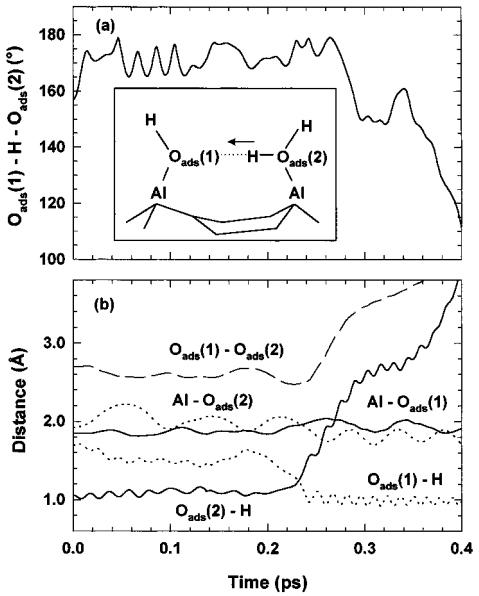

Figure 12. Time dependence of selected $O_{ads}-H-O_{ads}$ angle (a) and $O_{ads}-O_{ads}$, $Al-O_{ads}$, and $O_{ads}-H$ distances (b) associated with "proton diffusion" reaction observed during simulation begun with eight H_2O molecules (per supercell) in vicinity of one additional H_2O already dissociated (in 1−4 state). Inset to (a) shows schematic geometry of reacting species, with arrow showing the direction of proton transfer.

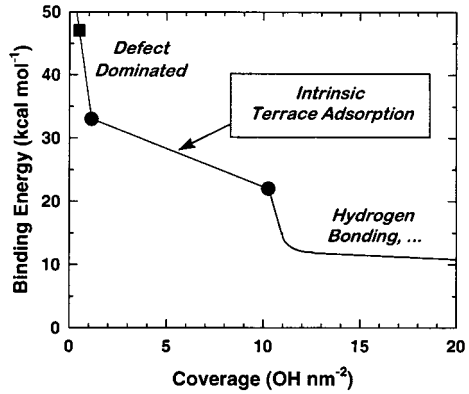

Figure 13. Estimated coverage dependence of H_2O binding energies on α-Al_2O_3 (0001) assuming a linear decrease between calculated points (filled circles, corresponding to one and nine H_2O molecules per supercell) in intrinsic region. Calculated binding energy for disrupted cluster geometry in Figure 4(b) (filled square) placed arbitrarily in defect-dominated regime. Large coverage limit fixed by H_2O heat of vaporization.

and dissociative adsorption decrease slightly with coverage, (2) dissociative adsorption remains favored, at least up to nine H_2O per supercell (one H_2O per surface Al), and (3) any surface Al atoms that descend into the surface near O_s-H sites (cf. Figures 2c and 2d) are pulled back out by the adsorption of H_2O on those Al. The most stable configuration with nine H_2O molecules per supercell is one in which all nine molecules are dissociated. Each surface Al in this case has an $O_{ads}-H$ group attached, and one out of every three oxygen atoms in the next layer has an attached proton and is part of an O_s-H group. An optimized 1×1 ordered arrangement yields an average adsorption energy per H_2O molecule of 27.5 kcal mol^{-1}. Comparison to the 33 kcal mol^{-1} found in section 3A for a single dissociatively adsorbed H_2O per supercell allows us to estimate the rate of decrease. Experimentally, decreasing H_2O binding energies have been observed in a variety of microcalorimetric[21−25,29,30] and laser and thermal desorption[15] measurements on α-Al_2O_3, but it is usually difficult to distinguish between intrinsic adsorption on a (0001) terrace and other types of adsorption, especially for powdered and nanocrystalline samples.

The general variation we expect in H_2O binding energies, based on our calculated results and an assumed linear decrease for intrinsic adsorption, is sketched in Figure 13. Unusually high binding energy sites associated with point defects (e.g., oxygen vacancies), steps,[38] and other deviations from an ideal Al-terminated (0001) surface will be preferentially occupied by the first molecules to adsorb; we assume the 47 kcal mol^{-1} binding energy we found for the disrupted cluster geometry in Figure 4a to be typical of this regime. Once defect sites are no longer available, an intrinsic adsorption region follows up to a coverage of about 10.3 OH per nm^2 (2 OH per surface Al), at which point all surface Al sites on (0001) terraces are likely to contain adsorbed $O_{ads}-H$ groups. The binding energy then falls off rapidly as any additional H_2O will either bind to surface Al that is already hydroxylated, to interior Al sites (which cannot occur without a significant local reconstruction), or to existing surface hydroxyl groups. At the very highest coverages, the H_2O binding energy asymptotically approaches the heat of vaporization of water[29] (10.5 kcal mol^{-1}) as the H_2O adlayer thickens and the only possibilities for binding are through hydrogen bonds to preadsorbed OH or H_2O.

Behavior qualitatively similar to that in Figure 13 has been observed experimentally in a microcalorimetry study[30] of nanocrystalline α-Al_2O_3. Particularly striking is the existence of sharp transition regions below about 4 OH per nm^2 and above 10 OH per nm^2. Measured binding energies in the intermediate regime that we associate with intrinsic terrace adsorption are about 10 kcal mol^{-1} higher in ref 30 than in Figure 13, but the slopes are similar. Recent desorption experiments[15(b)] on single-crystal α-Al_2O_3 (0001) surfaces yield somewhat lower intrinsic binding energies (23 to 41 kcal mol^{-1}), in better quantitative agreement with our predictions. Complementary adsorption experiments[15(a)] reveal a monotonically decreasing sticking coefficient, consistent with our predicted decrease in binding energies. The qualitative behavior in Figure 13 is further supported by a recent photoemission study[38] of the reaction of water vapor with α-Al_2O_3 (0001); the requirement that the H_2O partial pressure exceed a threshold of ∼1 Torr before significant hydroxylation occurs has been interpreted as evidence for a crossover from defect-site adsorption to intrinsic dissociative adsorption on (0001) terraces.[4,38]

C. Vibrational Frequencies. One of the most widely used methods for characterizing alumina surfaces is the spectroscopic analysis of O−H vibrational modes.[11,16−19,26,28,37] Using the approach described in section 2, we have estimated the frequencies of such modes for both molecularly adsorbed and dissociatively adsorbed H_2O from the H-atom trajectories in section 4A. The top part of Table 4 lists the results for O−H stretch frequencies after H_2O adsorption on Al-terminated α-Al_2O_3 (0001). For molecularly adsorbed H_2O, we also predict a $H-O_{ads}-H$ bending ("scissor") mode at ∼1625 cm^{-1}, which disappears upon dissociation. For a variety of reasons (e.g., inherent GGA inaccuracies,[77] limitations of our scale factor correction in section 2) we do not expect our frequency predictions to have better than a few percent accuracy. Comparisons to experiment are further complicated by the presence of defects, uncertain levels of hydration, and other factors that limit reproducibility. While these uncertainties make it difficult to test specific assignments of the closely spaced O−H peaks observed on many aluminas,[11,16−19] our calculated

TABLE 4: Estimated O−H Stretch Frequencies (in cm^{-1}) for Various Types of Surface Hydroxyl Species on α-Al_2O_3 (0001)

type of OH group	O coordination	frequency[a]
Al-terminated surface		
O_{ads}−H (molecularly adsorbed H_2O)	3	3450−3650
O_{ads}−H (dissociated H_2O)	2	3780
O_s−H (dissociated H_2O)	4	3430
OH−terminated surface		
O_s−H (free)	3	3650
O_s−H (hydrogen-bonded)	3	3470

[a] Calculated results scaled by 1.412 to account for fictitious electron mass, H → D substitution, and other computational details. Estimated uncertainty is several %.

frequencies do provide novel insights that advance the interpretation of experimental data[16,17,26,37] on α-Al_2O_3.

The results in Table 4 confirm the widely held belief that O−H stretch frequencies decrease with oxygen coordination number.[11,16−19] This trend is not surprising, given our finding in Table 2 that the corresponding O−H bond lengths increase. The highest frequency predicted, 3780 cm^{-1} for an O_{ads}−H hydroxyl group on surface Al, agrees exactly with a commonly observed peak on γ-Al_2O_3 that is usually assigned to a free hydroxyl group on an otherwise three-coordinated Al site.[11,16−19]

The predicted frequency range for molecularly adsorbed H_2O in Table 4 lies slightly below the symmetric (3657 cm^{-1}) and asymmetric (3756 cm^{-1}) stretching modes of isolated H_2O monomers.[77] This range is consistent with the usual assumption[16−19] that both molecularly adsorbed H_2O and hydrogen-bonded OH groups are responsible for the broad spectral features observed on many aluminas between 3300 and 3600 cm^{-1}. Intensities in this region tend to be highly sensitive to temperature and preparation conditions. On α-Al_2O_3, they can be reduced essentially to zero[16,37] by heating to 100−200 °C. This result and the complete absence of any spectroscopic signature for H−O_{ads}−H bending vibrations[16(b),26] strongly support our theoretical conclusion that any H_2O adsorbed on α-Al_2O_3 dissociates rapidly.

We expect H_2O dissociation on Al-terminated α-Al_2O_3 (0001) to produce two distinct O−H stretch peaks: one associated with O_{ads} (near 3780 cm^{-1}) and one with O_s (near 3430 cm^{-1}). Instead, both infrared[11] (IR) and electron-energy-loss[26,37] data for α-Al_2O_3 (0001) are dominated by a single peak at 3720−3733 cm^{-1}. While it is conceivable that the observed peak corresponds to our O_{ads}−H species (especially if its vibration is redshifted by hydrogen bonding to additional physisorbed H_2O), we do not find this explanation compelling in view of the sharpness and robustness of the observed peak and the absence of any additional sharp structure that could be associated with O_s−H.

A further hint that the picture of H_2O adsorption in sections 3 and 4 may be incomplete is provided by the isotope exchange experiments of Elam et al.[15(a)] These authors found that after exposing clean α-Al_2O_3 (0001) to $H_2{}^{18}O$, *both* $H_2{}^{16}O$ and $H_2{}^{18}O$ desorbed in essentially equal amounts. This effect obviously cannot be explained by a simple recombination of protons on O_s sites with $^{18}O_{ads}H$ groups produced by dissociation.

A resolution of these mysteries most likely requires a detailed understanding of the dynamical evolution of α-Al_2O_3 (0001) surfaces at still higher H_2O coverages and over much longer time scales than is currently possible with CPMD. Although such an undertaking is beyond the scope of the present paper, partial answers are provided by the additional CPMD results in the next section that support previous speculations[42,56,57,59] on the structure of heavily hydroxylated α-Al_2O_3 (0001).

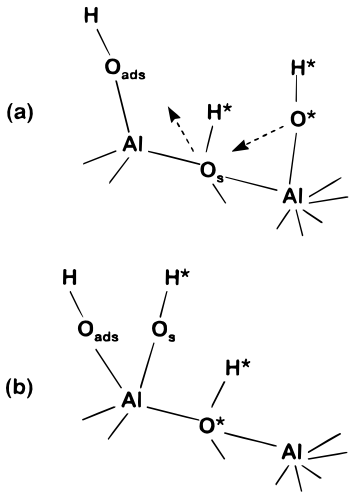

Figure 14. Schematic of atomic rearrangement observed in simulation begun with nine dissociated H_2O per supercell plus one additional $(H^*)_2O^*$ molecule dissociated on interior Al site (a). Arrows in (a) show direction of motion toward final state (b).

5. High H_2O Coverages

A. Disruption of Al-Terminated Surface. When the system in section 4B with nine dissociated H_2O molecules per supercell is allowed to evolve dynamically at ∼300 K, many of the surface Al−O_s bonds become highly strained and even break temporarily. Large lateral displacements within the outermost O layer make some interior Al sites more accessible to additional H_2O molecules than would be the case on a clean surface. Such molecules may either hydrogen bond to existing OH groups or bare O_s sites, interact with a surface Al on which there is already an O_{ads}−H group, or attempt to interact with interior Al.

We have not explored any of these possibilities systematically, but we did perform a few test simulations with nine dissociated plus one additional $(H^*)_2O^*$ molecule per supercell. In one case, in which we assumed that the additional molecule was also dissociated, with its residual O*−H* on a third-layer Al and its transferred proton on an adjacent O_s site, something very interesting occurred. The nearby atoms rearranged themselves so that the O*−H* replaced its neighboring O_s−H, while the latter tilted up and became a second singly coordinated hydroxyl group bound to a surface Al (cf. Figure 14). This rearrangement provides one possible pathway for the interchange of adsorbed (O*) and lattice (O_s) oxygen, the occurrence of which is implied by the isotopic-labeling experiments of ref 15. (Note that an $(H^*)_2O_s$ molecule might easily form and desorb after this rearrangement, but the O_s atom would not be readily available if the $(H^*)_2O^*$ molecule dissociated directly on surface Al.) It would be interesting to characterize all possible exchange processes in sufficient detail to explain why the observed ratio of $H_2{}^{18}O$ and $H_2{}^{16}O$ desorbing from a surface exposed to $H_2{}^{18}O$ is almost exactly 1:1.

The addition of multiple hydroxyl groups to surface Al, as in Figure 14b, raises the possibility of a massive disruption of the original Al-terminated surface.[57,60] Each OH group added further weakens the bonds between the Al and next-layer O (or OH). At very high H_2O coverages, it is likely that the surface Al will be etched away entirely in the form of hydrated Al$(OH)_3$ and related complexes (e.g., $Al(OH)_4$−), the exact form of which will depend on the pH, presence of impurities, and other conditions.[112] Whether Al etching can occur directly on

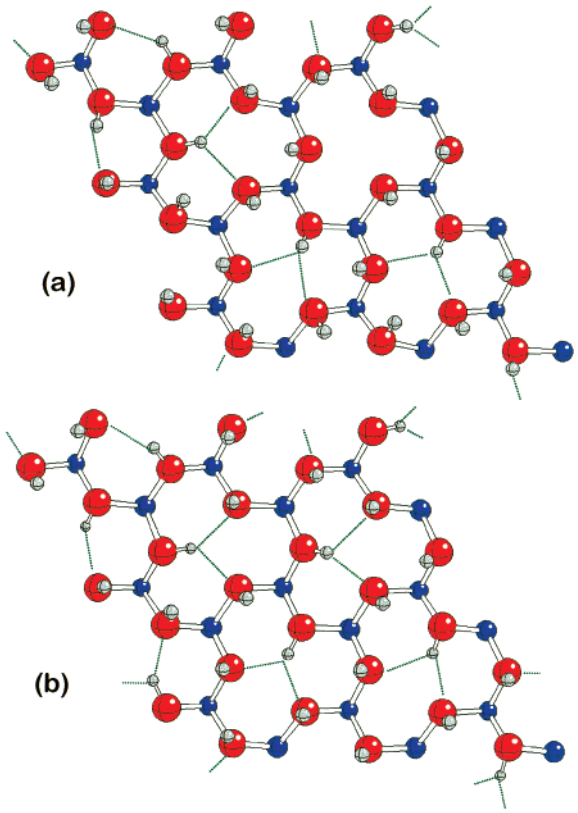

Figure 15. Instantaneous configurations of outermost layers of supercell model for OH-terminated α-Al_2O_3 (0001) at arbitrary time t^* (a) and $t^* + 0.15$ ps (b) during simulation at ~300 K. Colors same as in Figure 2. Dotted lines denote hydrogen bonds (defined by criterion that O−H distance < 2.4 Å).

ideal α-Al_2O_3 (0001) terrace regions, or whether it proceeds from step edges and other defects is unclear. The end result is a completely OH-terminated surface that differs from that in Figure 1 by the replacement of each surface Al with three protons. Such a surface is similar to that in the aluminum hydroxide minerals gibbsite and bayerite.[7,113] Thermodynamically, α-Al_2O_3 should transform completely to bulk $Al(OH)_3$ in the presence of an H_2O reservoir at room temperature,[7,39] but the kinetic barriers will be large once the surface is fully hydroxylated. IR evidence that the prolonged exposure of α-Al_2O_3 to H_2O does produce gibbsite- and bayerite-like surfaces has been reported by Lee and Condrate.[114] A very recent theoretical study provides further support for the above picture of the effects of heavy hydroxylation.[115]

B. OH-Terminated α-Al_2O_3 (0001). The possibility of uniform OH-termination of α-Al_2O_3 (0001) has been proposed in a number of earlier studies[42,56−60] and is often implicitly assumed in references to "oxygen termination" and discussions of alumina vibrational spectra.[11] Every Al in this model remains octahedrally coordinated, while every terminating OH group bridges two interior Al. The OH coordination is thus identical to that in bulk aluminum hydroxides (which consist of Al in two out of every three octahedral sites between close-packed OH layers), except that in the hydroxides, the OH groups contribute to structural integrity through interlayer hydrogen bonding.[7,9,113]

CPMD simulations for OH-terminated α-Al_2O_3 (0001) reveal a complex dynamical structure with extensive *intralayer* hydrogen bonding. Representative configurations separated by 0.15 ps during the same dynamics run at ~300 K are shown in Figure 15. On average, one out of every three hydroxyl groups lay nearly parallel to the surface and form long hydrogen bonds (H···O = 1.8−2.2 Å) to neighboring O sites across the regions where Al would be if the surface were Al-terminated. (Similar intralayer hydrogen bonding is also present in aluminum hydroxides.[7,9,113]) The other two out of three hydroxyls point nearly perpendicular to the surface and have a shorter average bond length (0.96 vs 0.98 Å).

In contrast to the large relaxation that occurs upon Al termination (section 3A), the outermost Al and O layers do not relax to any appreciable extent on OH-terminated α-Al_2O_3 (0001). A similar conclusion was drawn in a recent classical force-field study,[56] although the empirical potentials in that work failed to predict the tendency to form intralayer hydrogen bonds. With the exception of the H itself, the ordering of OH-terminated α-Al_2O_3 (0001) is essentially 1 × 1, making it difficult to distinguish this surface from Al-terminated α-Al_2O_3 (0001) in diffraction experiments.[15,35]

The large lateral extents of our supercells allow the surface hydroxyl groups in our simulations to exhibit complex patterns of hydrogen bonding. These patterns tend to lock in on the scale of ~0.1 ps, but evolve over longer periods (e.g., from (a) to (b) in Figure 15), even at 300 K. During a lock-in period, the out-of-plane H exhibits larger mean-square displacements than in-plane H (~0.15 vs ~0.10 $Å^2$/atom), with the dominant motion in the two cases being parallel to and perpendicular to the surface, respectively.

Differences between free and hydrogen-bonded hydroxyls also manifest themselves in different contributions to O−H vibrational spectra.[60] In our calculations, the former produce a fairly narrow peak at ~3650 cm^{-1}, while the latter produce a broader peak, with about half the integrated intensity, at ~3470 cm^{-1} (cf. Table 4). Although we cannot rule out the possible importance of defect structures, we believe that free hydroxyl vibrations on an OH-terminated surface provide the most likely explanation for the sharp 3720−3733 cm^{-1} peak that dominates experimental spectra[11,26,37] for α-Al_2O_3. Standard assignments for bridging-OH groups on aluminas[11,16−19] and scaled HF results for alumina cluster models[57,58] support this explanation. (A relatively large quantitative error in the predicted free hydroxyl frequency could be partly an artifact of our scaling procedure.)

The above explanation also predicts a red-shifted, hydrogen-bonded OH contribution, which tends not to be observed as a well-defined peak in experiments on single-crystal α-Al_2O_3 (0001). We expect this contribution to be extremely broad and weak because of the hydrogen bonding,[66(b)] the smaller number of contributing O−H groups, and selection-rule considerations that make it difficult to observe in-plane vibrations.[116] The existence of two distinct frequency regimes for OH-terminated α-Al_2O_3 (0001) points to a deficiency in the standard alumina classification schemes.[11,16−19] These schemes assume that all O−H groups with the same O and neighboring Al coordination numbers (e.g., all O−H groups in Figure 15) have the same frequency. Clearly, longer-range environmental effects, such as hydrogen bonding, limit the validity of this assumption.

Complete OH termination yields a coverage of 15 OH per nm^2 and should provide high physical and chemical stability.[56,60] Simulations at elevated temperatures (up to 600 K) showed no tendency for surface hydroxyl groups to combine and desorb as H_2O. (At sufficiently high temperatures, of course, H_2O will desorb, leaving a defective surface that bears no resemblence to the original Al-terminated state.) Any additional H_2O coming into contact with the surface can only adsorb molecularly by hydrogen bonding to surface O and/or H. OH-terminated

α-Al_2O_3 (0001) will be much less reactive than, and the chemistry will be entirely different from what occurs on, Al-terminated α-Al_2O_3 (0001). These two terminations, in fact, probably represent the most extreme contrast in chemical behavior that exists among alumina surfaces. Such a contrast reinforces the belief that careful surface preparation and characterization (especially the state of hydroxylation) are essential in any meaningful experimental investigation of alumina surface chemistry.

6. Conclusions

The increasing tractability of first-principles molecular dynamics simulations opens a new window into the microscopic behavior of complex oxide surfaces. The present application to large supercell models of α-Al_2O_3 (0001) has elucidated many aspects of the static and dynamical properties of adsorbed H_2O over a wide range of coverages. An alternative small-cluster-model description is quantitatively unreliable and produces artifacts in some cases because of its finite lateral extent.

The ideal Al-terminated surface is highly reactive to H_2O dissociation, making it extremely difficult in practice to achieve a completely unhydroxylated surface. H_2O adsorption produces significant changes in the local geometry near surface Al sites; in particular, it pulls the Al out from its highly relaxed position on a clean surface. Details of specific dissociation and other proton-transfer reactions have been explored via free-energy profiles and/or direct simulations. Dissociation into a "1−4" state is strongly favored kinetically over a competing "1−2" pathway and can also be mediated by a second H_2O molecule that participates in a concerted exchange of two protons. The predicted coverage dependence of the H_2O binding energy is in reasonable agreement with experiment, but the observed O−H vibrational spectrum is *inconsistent* with expectations for a hydroxylated Al-terminated surface.

It is likely that this discrepancy results from the etching of surface Al at high H_2O coverages. The resulting OH-terminated surface is highly stable, in better agreement with observed vibrational spectra, and surprisingly complex because of extensive and dynamic in-plane hydrogen bonding. Details of the transformation pathways between Al- and OH-terminated α-Al_2O_3 (0001), and many other unresolved issues in alumina surface chemistry, are ripe for further theoretical and experimental investigation.

Acknowledgment. Most of the computer time used in this work was provided by the IBM Thomas J. Watson Research Laboratory (Yorktown Heights, New York). Two of us (K.C.H. and W.F.S.) thank the authors of references 15, 32, 55, 57, and 58 for communicating their results prior to publication.

References and Notes

(1) Henrich, V. E.; Cox, P. A. *The Surface Science of Metal Oxides*; Cambridge University Press: Cambridge, 1994.

(2) Noguera, C. *Physics and Chemistry at Oxide Surfaces*; Cambridge University Press: Cambridge, 1996.

(3) Freund, H.-J.; Kuhlenbeck, H.; Staemmler, V. *Rep. Prog. Phys.* **1996**, *59*, 283.

(4) Brown, G. E.; Henrich, V. E.; Casey, W. H.; Clark, D. L.; Eggleston, C.; Felmy, A.; Goodman, D. W.; Grätzel, M.; Maciel, G.; McCarthy, M. I.; Nealson, K. H.; Sverjensky, D. A.; Toney, M. F.; Zachara, J. M. *Chem. Rev.* **1999**, *99*, 77.

(5) Catlow, C. R. A.; Freeman, C. M.; Islam, M. S.; Jackson, R. A.; Leslie, M.; Tomlinson, S. M. *Philos. Mag. A* **1988**, *58*, 123.

(6) Vanderbilt, D. *Phys. Rev. B* **1990**, *41*, 7892.

(7) Wefers, K.; Misra, C. *Alcoa Technical Paper 19 (revised);* Alcoa Laboratories: St. Louis, 1987.

(8) Levin, I.; Brandon, D. *J. Am. Ceram. Soc.* **1998**, *81*, 1995.

(9) Hsu, P. H. In *Minerals in Soil Environments*; Dixon, J. B., Weed, S. B., Eds.; Soil Science Society of America: Madison, WI, 1989; p 331.

(10) Lippens, B. C.; Steggerda, J. J. In *Physical and Chemical Aspects of Adsorbents and Catalysts*; Linsen, B. G., Ed.; Academic: New York, 1970; p 171.

(11) Knözinger, H.; Ratnasamy, P. *Catal. Rev. − Sci. Eng.* **1978**, *17*, 31.

(12) French, R. H., Ed. *J. Am. Ceram. Soc.* **1994**, *77*.

(13) Kinloch, A. J. *Adhesion and Adhesives: Science and Technology*; Chapman and Hall: London, 1987.

(14) Eisenberger, P. M., Ed.; *Basic Research Needs for Vehicles of the Future*; Princeton Materials Institute: Princeton, 1995.

(15) Elam, J. W.; Nelson, C. E.; Cameron, M. A.; Tolbert, M. A.; George, S. M. *J. Phys. Chem. B* **1998**, *102*, 7008. (b) Nelson, C. E.; Elam, J. W.; Cameron, M. A.; Tolbert, M. A.; George, S. M. *Surf. Sci.* **1998**, *416*, 341.

(16) Morterra, C.; Ghiotti, G.; Garrone, E.; Boccuzzi, F. *J. Chem. Soc., Faraday Trans.* **1976**, *72*, 2722. (b) Morterra, C.; Magnacca, G.; Cerrato, G.; Del Favero, N.; Filippi, F.; Folonari, C. V. *J. Chem. Soc., Faraday Trans.* **1993**, *89*, 135. (c) Morterra, C.; Magnacca, G. *Catal. Today* **1996**, *27*, 497.

(17) Lygin, V. I.; Muzyka, I. S. *Russ. J. Phys. Chem.* **1995**, *69*, 1829.

(18) Tsyganenko, A. A.; Mardilovich, P. P. *J. Chem. Soc., Faraday Trans.* **1996**, *92*, 4843. (b) Tsyganenko, A. A.; Mirnov, K. S. S.; Rzhevskij, A. M.; Mardilovich, P. P. *Mater. Chem. Phys.* **1990**, *26*, 35.

(19) Liu, X.; Truitt, R. E. *J. Am. Chem. Soc.* **1997**, *119*, 9856.

(20) Ahn, J.; Rabalais, J. W. *Surf. Sci.* **1997**, *388*, 121.

(21) Wade, W. H.; Hackerman, N. *J. Phys. Chem.* **1960**, *64*, 1196. (b) Venable, R. I.; Wade, W. H.; Hackerman, N. *J. Phys. Chem.* **1965**, *69*, 317.

(22) Peri, J. B.; Hannan, R. B. *J. Phys. Chem.* **1960**, *64*, 1526. (b) Peri, J. B. *J. Phys. Chem.* **1965**, *69*, 211.

(23) Yao, Y.-F. Y. *J. Phys. Chem.* **1965**, *69*, 3930.

(24) Hendriksen, B. A.; Pearce, D. R.; Rudham, R.; *J. Catal.* **1972**, *24*, 82.

(25) Gatta, G. D.; Fubini, B.; Stradella, L. *J. Chem. Soc., Faraday Trans.* **1977**, *73*, 1040.

(26) Chen, J. G.; Crowell, J. E.; Yates, J. T. *J. Chem. Phys.* **1986**, *84*, 5906.

(27) Thiel, P. A.; Madey, T. E. *Surf. Sci. Rep.* **1987**, *7*, 211.

(28) Frederick, B. G.; Apai, G.; Rhodin, T. N. *Surf. Sci.* **1991**, *244*, 67.

(29) Rossi, P. F.; Oliveri, G.; Bassoli, M. *J. Chem. Soc., Faraday Trans.* **1994**, *90*, 363.

(30) McHale, J. M.; Navrotsky, A. *J. Phys. Chem. B* **1997**, *101*, 603. (b) McHale, J. M., Auroux, A.; Perrotta, A. J.; Navrotsky, A. *Science* **1997**, *277*, 788.

(31) Soled, S. *J. Catal.* **1983**, *81*, 252.

(32) Sohlberg, K.; Pennycook, S. J.; Pantelides, S. T. *J. Am. Chem. Soc.* **1999**, *121*, 7493.

(33) French, T. M.; Somorjai, G. A. *J. Phys. Chem.* **1970**, *74*, 2489.

(34) Liehr, M.; Thiry, P. A.; Pireaux, J. J.; Caudano, R. *J. Vac. Sci. Technol. A* **1984**, *2*, 1079.

(35) Gautier, M.; Renaud, G.; Van, L. P.; Villette, B.; Pollak, M.; Thromat, N.; Jollet, F.; Duraud, J.-P. *J. Am. Ceram. Soc.* **1994**, *77*, 323.

(36) Guenard, P.; Renaud, G.; Barbier, A.; Gautier-Soyer, M. *Mater. Res. Soc. Symp. Proc.* **1996**, *437*, 15.

(37) Coustet, V.; Jupille, J. *Surf. Sci.* **1994**, *307−309*, 1161. (b) Coustet, V.; Jupille, J. *Surf. Interface Anal.* **1994**, *22*, 280. (c) Coustet, V.; Jupille, J.; *Nuovo Cimento* **1997**, *19*, 1657.

(38) Heffelfinger, J. R.; Bench, M. W.; Carter, C. B. *Surf. Sci.* **1997**, *370*, L168.

(39) Liu, P.; Kendelewicz, T.; Brown, G. E.; Nelson, E. J.; Chambers, S. A. *Surf. Sci.* **1998**, *417*, 53.

(40) Toofan, J.; Watson, P. R. *Surf. Sci.* **1998**, *401*, 162.

(41) Ciraci, S.; Batra, I. P. *Phys. Rev. B* **1983**, *28*, 982.

(42) Pushkarchuk, A. L.; Mardilovich, P. P.; Trokhimets, A. L.; Zhidomirov, G. M.; Gagarin, S. G. *Phys. Status Solidi B* **1984**, *124*, 699. (b) Pushkarchuk, A. L.; Mardilovich, P. P.; Trokhimets, A. L.; Gagarin, S. G.; Zhidomirov, G. M. *Phys. Status Solidi B* **1985**, *129*, K181.

(43) Pisani, C.; Causà, M.; Dovesi, R.; Roetti, C. *Prog. Surf. Sci.* **1987**, *25*, 119. (b) Causà, M.; Dovesi, R.; Pisani, C.; Roetti, C. *Surf. Sci.* **1989**, *215*, 259.

(44) Mackrodt, W. C. *J. Chem. Soc., Faraday Trans.* **1989**, *85*, 541. (b) Mackrodt, W. C. *Philos. Trans. Royal Soc. A* **1992**, *341*, 301.

(45) Guo, J.; Ellis, D. E.; Lam, D. J. *Phys. Rev. B* **1992**, *45*, 13647.

(46) Ilchenko, N. N.; Gorb, L. G.; Goncharuk, V. V. *Surf. Sci.* **1992**, *274*, 287. (b) Gorb, L. G.; Ilchenko, N. N.; Goncharuk, V. V. *J. Mol. Catal. A* **1995**, *98*, 147.

(47) Blonski, S.; Garofalini, S. H. *Surf. Sci.* **1993**, *295*, 263. (b) Blonski, S.; Garofalini, S. H. *J. Phys. Chem.* **1996**, *100*, 2201.

(48) Manassidis, I.; De Vita, A.; Gillan, M. J. *Surf. Sci.* **1993**, *285*, L517. (b) Manassidis, I.; Gillan, M. J. *J. Am. Ceram. Soc.* **1994**, *77*, 335.

(49) Godin, T. J.; LaFemina, J. P. *Phys. Rev. B* **1994**, *49*, 7691.

(50) Streitz, F. H.; Mintmire, J. W. *Phys. Rev. B* **1994**, *50*, 11996. (b) Streitz, F. H.; Mintmire, J. W. *Thin Solid Films* **1994**, *253*, 179.
(51) Frank, I.; Marx, D.; Parrinello, M. *J. Am. Chem. Soc.* **1995**, *117*, 8037. (b) Frank, I.; Marx, D.; Parrinello, M. *J. Chem. Phys.* **1996**, *104*, 8143.
(52) Puchin, V. E.; Gale, J. D.; Shluger, A. L.; Kotomin, E. A.; Günster, J.; Brause, M.; Kempter, V. *Surf. Sci.* **1997**, *370*, 190.
(53) Verdozzi, C.; Jennison, D. R.; Schultz, P. A.; Sears, M. P. *Phys. Rev. Lett.* **1999**, *82*, 799.
(54) Batirev, I. G.; Alavi, A.; Finnis, M. W.; Deutsch, T. *Phys. Rev. Lett.* **1999**, *82*, 1510.
(55) Ruberto, C.; Yourdshahyan, Y.; Lundqvist, B. I., unpublished.
(56) Nygren, M. A.; Gay, D. H.; Catlow, C. R. A. *Surf. Sci.* **1997**, *380*, 113.
(57) Wittbrodt, J. M.; Hase, W. L.; Schlegel, H. B. *J. Phys. Chem. B* **1998**, *102*, 6539.
(58) Kubicki, J. D.; Apitz, S. E. *Am. Mineral.* **1998**, *83*, 1054.
(59) de Leeuw, N. H.; Parker, S. C. *J. Am. Ceram. Soc.* **1999**, *82*, 3209.
(60) Hass, K. C.; Schneider, W. F.; Curioni, A.; Andreoni; W. *Science* **1998**, *282*, 265.
(61) Car, R.; Parrinello, M. *Phys. Rev. Lett.* **1985**, *55*, 2471.
(62) Galli, G.; Parrinello, M. In *Computer Simulation in Materials Science*; Meyer, M., Pontikis, V., Eds.; Kluwer Academic: Dordrecht, 1991.
(63) Parr, R. G.; Yang, W. *Density Functional Theory of Atoms and Molecules*; Oxford University Press: Oxford, 1989.
(64) Payne, M. C.; Teter, M. P.; Allan, D. C.; Arias, T. A.; Joannopoulos, J. D. *Rev. Mod. Phys.* **1992**, *64*, 1045.
(65) For examples, see the selected reviews by (a) Tuckerman, M. E.; Ungar, P. J.; von Rosenvinge, T.; Klein, M. L. *J. Phys. Chem.* **1996**, *100*, 12878, and (b) Parrinello, M. *Solid State Commun.* **1997**, *102*, 107.
(66) Langel, W.; Parrinello, M. *Phys. Rev. Lett.* **1994**, *73*, 504. (b) Langel, W.; Parrinello, M. *J. Chem. Phys.* **1995**, *103*, 3240. (c) Langel, W. *Chem. Phys. Lett.* **1996**, *259*, 7.
(67) Refson, K.; Wogelius, R. A.; Fraser, D. G.; Payne, M. C.; Lee, M. H.; Milman, V. *Phys. Rev. Lett.* **1995**, *52*, 10823.
(68) Szymanski, M. A.; Gillan, M. J. *Surf. Sci.* **1996**, *367*, 135. (b) Kantorovich, L. N.; Gillan, M. J. *Surf. Sci.* **1997**, *374*, 373.
(69) Giordano, L.; Goniakowski, J.; Suzanne, J. *Phys. Rev. Lett.* **1998**, *81*, 1271.
(70) Odelius, M. *Phys. Rev. Lett.* **1999**, *82*, 3919.
(71) Goniakowski, J.; Gillan, M. J. *Surf. Sci.* **1996**, *350*, 145. (b) Lindan, P. J. D.; Harrison, N. M.; Holender, J. M.; Gillan, M. J. *Chem. Phys. Lett.* **1996**, *261*, 246. (c) Lindan, P. J. D.; Harrison, N. M.; Gillan, M. J. *Phys. Rev. Lett.* **1998**, *80*, 762. (d) Bates, S. P.; Gillan, M. J.; Kresse, G. *J. Phys. Chem. B* **1998**, *102*, 2017. (e) Bates, S. P.; Kresse, G.; Gillan, M. J. *Surf. Sci.* **1998**, *409*, 336.
(72) Vittadini, A.; Selloni, A.; Rotzinger, F. P.; Grätzel, M. *Phys. Rev. Lett.* **1998**, *81*, 2954. (b) Selloni, A.; Vittadini, A.; Grätzel, M. *Surf. Sci.* **1998**, *402*−*404*, 219.
(73) Kantorovich, L. N.; Gillan, M. J. *Surf. Sci.* **1997**, *376*, 169.
(74) Becke, A. D. *Phys. Rev. A* **1988**, *38*, 3098.
(75) Lee, C.; Yang, W.; Parr, R. *Phys. Rev. B* **1988**, *37*, 785.
(76) Sprik, M.; Hutter, J.; Parrinello, M. *J. Chem. Phys.* **1996**, *105*, 1142.
(77) Johnson, B. G.; Gill, P. M. W.; Pople, J. A. *J. Chem. Phys.* **1993**, *98*, 5612.
(78) Troullier, N.; Martins, J. L. *Phys. Rev. B* **1991**, *43*, 1993.
(79) Kleinman, L.; Bylander, D. M. *Phys. Rev. Lett.* **1982**, *48*, 1425.
(80) Curioni, A.; Boero, M.; Andreoni, W. *Chem. Phys. Lett.* **1998**, *294*, 263.
(81) Barnett, R. N.; Landman, U. *Phys. Rev. B* **1993**, *48*, 2081.
(82) Hutter, J.; Lüthi, H. P.; Parrinello, M. *Comput. Mater. Sci.* **1994**, *2*, 244.
(83) Fischer, Th. H.; Amlöf, J. *J. Phys. Chem.* **1992**, *96*, 9768.
(84) Allen, M. P.; Tildesley, D. J. *Computer Simulation of Liquids*; Clarendon Press: Oxford, 1987.
(85) Marx, D.; Parrinello, M. *J. Chem. Phys.* **1996**, *104*, 4077. (b) Tuckerman, M. E.; Marx, D.; Klein, M. L.; Parrinello, M. *J. Chem. Phys.* **1996**, *104*, 5579.
(86) Tuckerman, M. E.; Marx, D.; Klein, M. L.; Parrinello, M. *Science* **1997**, *275*, 817. (b) Marx, D.; Tuckerman, M. E.; Hutter, J.; Parrinello, M. *Nature* **1999**, *397*, 601.
(87) Nosé, S. *J. Chem. Phys.* **1984**, *81*, 511.
(88) Hoover, W. G. *Phys. Rev. A* **1985**, *31*, 1695.
(89) Ciccotti, G.; Ferrario, M.; Hynes, J. T.; Kapral, R. *Chem. Phys.* **1989**, *129*, 241. (b) Carter, E. A.; Ciccotti, G.; Hynes, J. T.; Kapral, R. *Chem. Phys. Lett.* **1989**, *156*, 472. (c) Sprik, M.; Ciccotti, G. *J. Chem. Phys.* **1998**, *109*, 7737.
(90) Curioni, A.; Sprik, M.; Andreoni, W.; Schiffer, H.; Hutter, J.; Parrinello, M. *J. Am. Chem. Soc.* **1997**, *119*, 721.
(91) Trout, B. L.; Parrinello, M. *Chem. Phys. Lett.* **1998**, *288*, 343. (b) Trout, B. L.; Parrinello, M. *J. Phys. Chem. B* **1999**, *103*, 7340.
(92) Tasker, P. W. *Adv. Ceram.* **1988**, *10*, 176.
(93) Wang, X.-G.; Weiss, W.; Shaikhutdinov, Sh. K.; Ritter, M.; Petersen, M.; Wagner, F.; Schlögl, R.; Scheffler, M. *Phys. Rev. Lett.* **1998**, *81*, 1038.
(94) Perdew, J. P.; Burek, K.; Ernzerhof, M. *Phys. Rev. Lett.* **1996**, *77*, 3865.
(95) Perdew, J. P.; Chevary, J. A.; Vosko, S. H.; Jackson, K. A.; Pederson, M. R.; Singh, D. J.; Fiolhais, C. *Phys. Rev. B* **1982**, *46*, 6671.
(96) Somorjai, G. A.; Van Hove, M. A. *Prog. Surf. Sci.* **1991**, *30*, 201.
(97) Becke, A. D. *J. Chem. Phys.* **1993**, *98*, 5648.
(98) Anchell, J. L.; Hess, A. C. *J. Phys. Chem.* **1996**, *100*, 18317.
(99) Lü, X.; Xu, X.; Wang, N.; Zhang, Q.; Ehara, M.; Nakatsuji, H. *Chem. Phys. Lett.* **1998**, *291*, 445.
(100) Hass, K. C.; Schneider, W. F. *Phys. Chem. Chem. Phys.* **1999**, *1*, 639.
(101) Scheiner, S. In *Proton Transfer in Hydrogen-Bonded Systems*; Bountis, T., Ed.; Plenum: New York, 1992; p 29.
(102) Johnson, B. G.; Gonzales, C. A.; Gill, P. M. W.; Pople, J. A. *Chem. Phys. Lett.* **1994**, *221*, 100.
(103) Repelin, Y.; Husson, E.; Proust, C. *J. Solid State Chem.* **1995**, *116*, 378.
(104) Brown, D. E.; Moffatt, D. J.; Wolkow, R. A. *Science* **1998**, *279*, 542.
(105) Antonczak, S.; Ruiz-López, M. F.; Rivail, J. L.; *J. Am. Chem. Soc.* **1994**, *116*, 3914.
(106) Morokuma, K.; Muguruma, C. *J. Am. Chem. Soc.* **1994**, *116*, 10316.
(107) Bell, R. L.; Troung, T. N. *J. Chem. Phys.* **1994**, *101*, 10442.
(108) Schneider, W. F.; Wallington, T. J.; Huie, R. E.; *J. Phys. Chem.* **1996**, *100*, 6097.
(109) Aida, M.; Yamataka, H.; Dupuis, M. *Chem. Phys. Lett.* **1998**, *292*, 474.
(110) Meijer, E. J.; Sprik, M. *J. Phys. Chem. A* **1998**, *102*, 2893−2898.
(111) Huggins, B. A.; Ellis, P. D. *J. Am. Chem. Soc.* **1992**, *114*, 2098.
(112) Ruiz, J. M.; McAdon, M. H.; Garcés, J. M. *J. Phys. Chem. B* **1997**, *101*, 1733.
(113) Russell, J. D.; Parfitt, R. L.; Fraser, A. R.; Farmer, V. C. *Nature* **1974**, *248*, 220.
(114) Lee, D. H.; Condrate, R. A. *Mater. Lett.* **1995**, *23*, 241.
(115) Di Felice, R.; Northrup, J. E. *Phys. Rev.* **1999**, *60*, R16287.
(116) Brown, W. A.; Gardner, P.; King, D. A. *J. Phys. Chem.* **1995**, *99*, 7065.